Preprint

A paradox promoted by microglia cannibalism shortens the lifespan of developmental microglia

Hannah Gordon,[1,2] Zachary T. Schafer[1], and Cody J. Smith[1,2]*

1 Department of Biological Sciences, 2 The Center for Stem Cells and Regenerative Medicine[2] at the University of Notre Dame, Notre Dame, IN.

*Cody J. Smith, csmith67@nd.edu

ABSTRACT:

The overproduction of cells and subsequent production of debris is a universal principle of neurodevelopment. Here we show an additional feature of the developing nervous system that causes neural debris – promoted by the sacrificial nature of embryonic microglia that irreversibly become phagocytic after clearing other neural debris. Described as long-lived, microglia colonize the embryonic brain and persist into adulthood. Using transgenic zebrafish to investigate the microglia debris during brain construction, we identified that unlike other neural cell-types that die in developmental stages after they have expanded, necroptotic-dependent microglial debris is prevalent when microglia are expanding in the zebrafish brain. Time-lapse imaging of microglia demonstrates that this debris is cannibalized by other microglia. To investigate features that promote microglia death and cannibalism, we used time-lapse imaging and fate-mapping strategies to track the lifespan of individual developmental microglia. These approaches revealed that instead of embryonic microglia being long-lived cells that completely digest their phagocytic debris, once most developmental microglia in zebrafish become phagocytic they eventually die, including ones that are cannibalistic. These results establish a paradox -- which we tested by increasing neural debris and manipulating phagocytosis -- that once most microglia in the embryo become phagocytic, they die, create debris and then are cannibalized by other microglia, resulting in more phagocytic microglia that are destined to die.

MAIN TEXT:

Programmed cell death and clearance of that debris is a universal principle of nervous system development[1,2]. In vertebrates, this debris is cleared by microglia, which are the resident and professional phagocyte of the brain[3]. Microglia are considered long-lived cells that colonize the embryonic brain from the embryonic yolk-sac[3–7]. This definition is supported by fate-mapping studies that demonstrate yolksac derived cells generate microglia that persist into adulthood and intravital imaging of adult mouse brains that demonstrate low turnover of microglia in the healthy animals[5–8]. Conflicting the long-lived nature of microglia is evidence of microglia turnover in zebrafish and humans during development, and of microglia death in adult mice[9,10]. To understand the lifespan of microglia, we searched for microglia death during brain construction. Using zebrafish to precisely fate-map individual microglia, we found that once most embryonic microglia become phagocytic, they die. Unique from other cells in development, this death is necroptotic. The scale of this death requires a rapid turnover of microglia when they are expanding in the brain. Unlike the adult brain states when microglia are tiled[11], our evidence in zebrafish shows that developmental microglia cannibalize microglia debris, resulting in microglia that are destined to die because they are phagocytic. In addition to introducing a new process that produces developmental cell death, this work demonstrates that embryonic microglia lifespan rarely exceeds 3 days when phagocytic debris is prominent.

To explore microglia death in the developing nervous system, we first searched for signatures of microglia death in the developing brain using transgenic zebrafish, *Tg(pu1:gal4-uas:gfp)* (hereafter *pu1:gfp*) that use regulatory regions of *pu1* to label microglia populations[12]. To ensure that we could identify death regardless of the mode of death, we first scored the amount of GFP+ debris in the brain from 3-5 dpf. In these ages, we scored that GFP+ microglia debris was present and increased across days (Figure 1a,b. N=21 animals, p=0.0397 3 dpf vs 5 dpf, Post hoc Tukey Test). We confirmed this debris was derived from microglia and not from other *pu1+* macrophages that may enter the embryonic brain by demonstrating they also label with the zebrafish microglia-specific antibody 4C4 (Figure 1c)[13,14]. To investigate how this debris could occur, we generated movies of *Tg(pu1:gfp)* animals for 24 hours (Movie S1). While shedding of GFP+ debris from living microglia is a possibility, we never saw such an event in 24-hour movies. Instead, we could detect that GFP+ microglia debris was caused by microglia cell death (Figure S1c, n=10 cells).

Most developmental death is mediated by apoptosis[1]. To identify the molecular mechanism of this microglia death, we first treated animals with Z-VAD FMK, a pan caspase inhibitor that is highly effective at blocking apoptosis in multiple cell types[15]. To normalize the amount of debris per cell, we designed a strategy to label a specific number of microglia. To do this, we generated a *Tg(pu1:eos)* animal, which expresses the photoconvertible protein, Eos, in microglia (Figure 1d)[16]. In this paradigm, we exposed three microglia to 405 nm light and thereby photoconverted the Eos protein from green (488-Eos) to red (561-Eos) emission (Figure S1a). Scoring debris in DMSO vs Z-VAD FMK-treated animals was statistically indistinguishable (Figure 1e)(p=0.512 DMSO (n=12) vs Z-VAD-FMK(n=10), Dunnett's multiple comparisons test), indicating that the microglia death we identified is non-apoptotic and thereby distinct from the typical death that occurs in neurodevelopment. To identify the molecular mechanism of microglia debris, we then treated animals with
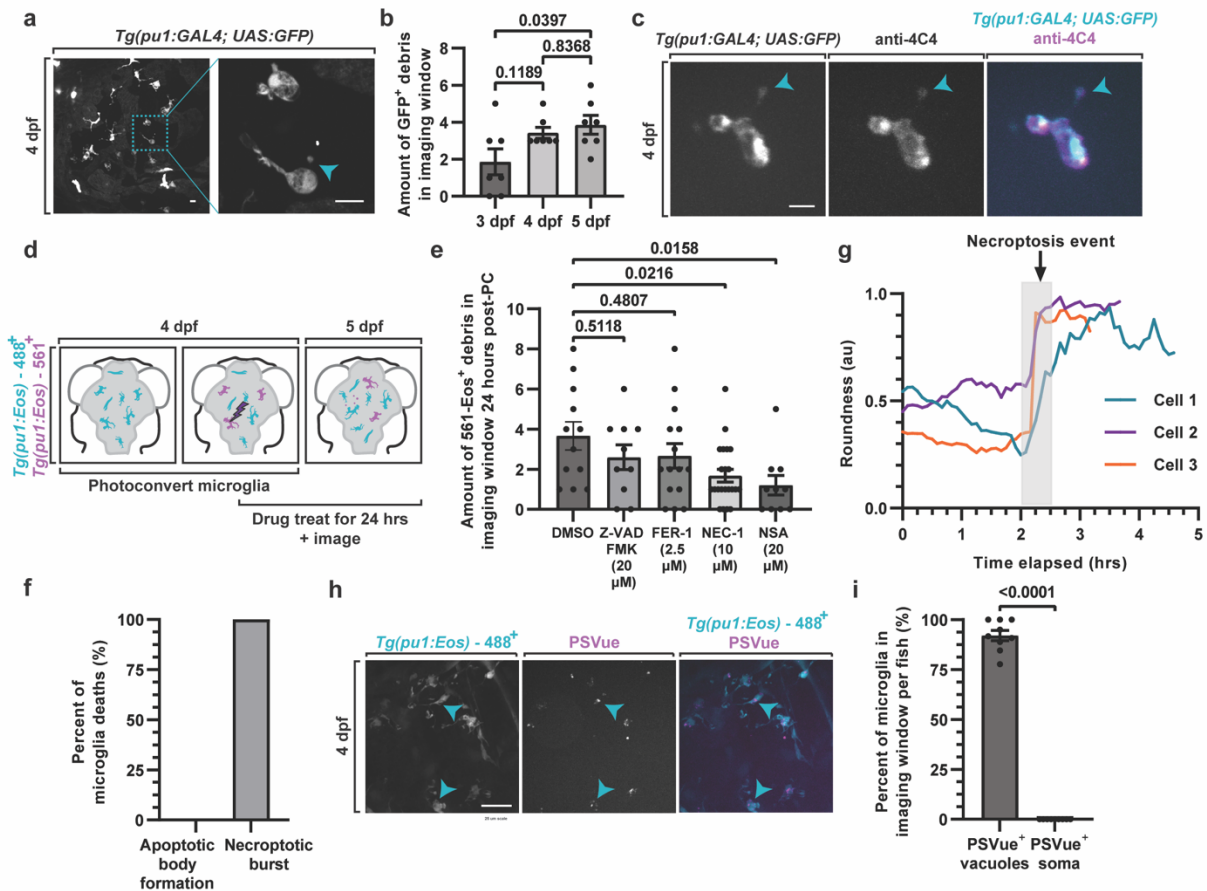
Figure 1. Microglia die via necroptosis in colonization stages. A-B. Confocal images of 4 dpf *Tg(pu1:GFP)* brains (A) and quantification (B) showing microglia debris (blue arrowhead) and intact microglia (p=0.1189 3 dpf vs 4 dpf, p=0.8368 4 dpf vs 5 dpf, p=0.0387 3 dpf vs 5 dpf, Post hoc Tukey test). C. Confocal images of 4 dpf *Tg(pu1:GFP)* brains labeled with anti-4C4 demonstrating GFP$^+$; 4C4$^+$ debris. D. Schematic of experimental paradigm (D) and quantification (E) of 561-Eos$^+$ debris in the brain 24-hour after labeling showing Nec-1 and NSA reduce microglia debris (p=0.5118 DMSO vs Z-VAD FMK, p=0.4807 DMSO vs Fer-1, p=0.0216 DMSO vs Nec-1 , p=0.0158 DMSO vs NSA, one-way ANOVA/Dunnett's multiple-comparisons test). F. Quantification of the percentage of microglia deaths in 24h timelapse movies that cause apoptotic bodies vs necroptotic burst. G. Quantification of cell roundness in a 24 h movie of microglia before it dies. H-I. Confocal images (H) and quantifications (I) of *Tg(pu1:Eos)* animals at 4 dpf that are treated with PsVue demonstrating PsVue labels vacuoles but not cell bodies (p<0.0001, unpaired t-test). Scale bar is 10 um (a, c, h). One-way ANOVA (b, e). Additional supplemental material provided in Figure S1. Descriptive statistics represented in Table S1.

inhibitors of ferroptosis (Fer-1) and necroptosis (Nec-1 and NSA)[17–19]. Treatment with necroptotic inhibitors, Nec-1 and NSA, reduced the amount of microglia debris while other inhibitors did not (Figure 1e)(p=0.0216 DMSO (n=12) vs Nec-1 (n=22), p=0.0158 DMSO (n=12) vs NSA (n=10), Dunnett's multiple comparisons test), consistent with the idea that embryonic microglia die via necroptosis.

To further understand if embryonic microglia death was necroptotic and not just dependent on other necroptotic cells, we visualized microglia as they undergo death with *Tg(pu1:gfp)* animals in 24 hour time-lapse movies. We scored the dynamic features of apoptotic cellular bodies that would be consistent with apoptosis[12,20,21]. In contrast, a rounding up of a cell followed by sudden disappearance of cytoplasmic labeling would be indicative of necroptosis[22]. Tracing of individual microglia every 5 minutes for 24 hours revealed that microglia death did not

exhibit apoptotic cellular bodies (Figure 1f, N=5 animals, n=10 cells). Instead, every microglia that died halted their migration, retracted all of their cellular processes to reduce their area, rounded up and then shortly later, burst (Figure 1g,f). We further identified that microglia membrane does not label with the phosphatidylserine reporter PSVue (Figure 1h,i, N=9 animals, n=92 cells), which is normally localized on apoptotic cells[23,24]. Together with the pharmacological inhibition, this strongly supports the idea that developmental microglia die via necroptosis.

To next investigate cell biological features that promote this microglia necroptosis, we tracked the lifespan of individual microglia until they died. To do this we utilized time-lapse imaging of the zebrafish brain to track individual microglia. In 4 dpf *Tg(pu1:gfp)* animals, we could detect microglia with cytosolic GFP labeling that contained GFP$^-$ vacuole-like
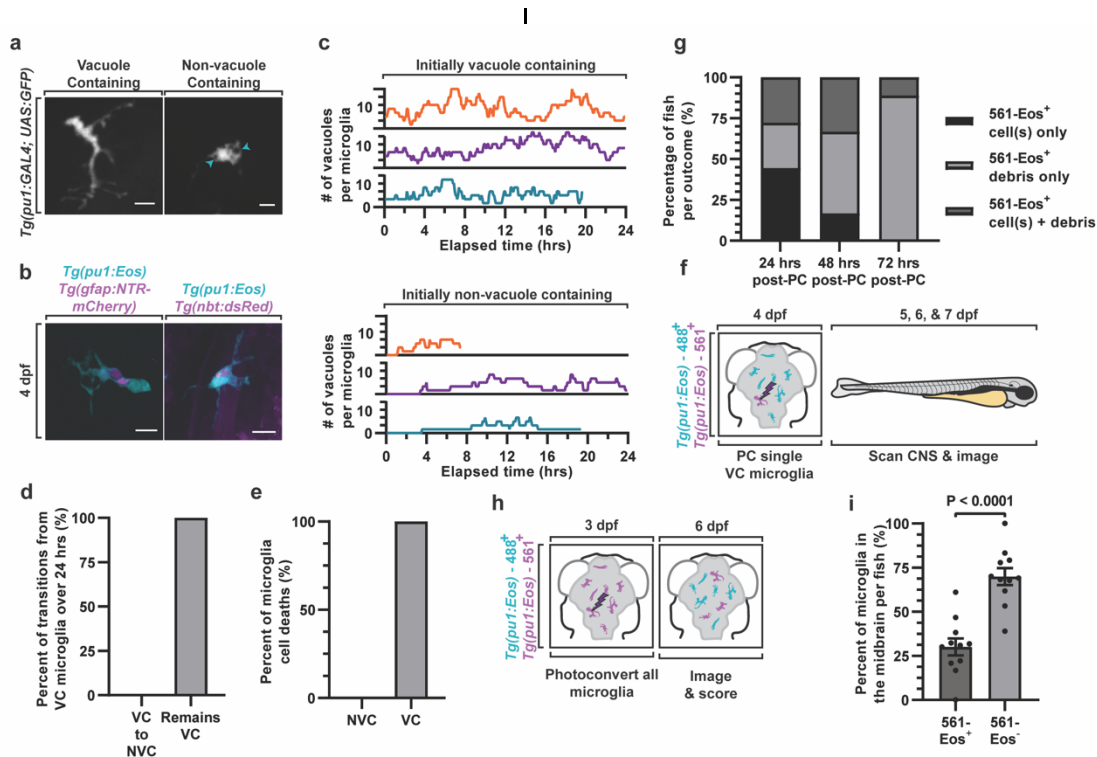
Figure 2. Developmental microglia have short lifespans after becoming vacuole-containing. A. Confocal images from a 24h timelapse movie showing microglia in *Tg(pu1:gfp)* animals that contain vacuoles and microglia that do not have vacuoles. B. Confocal images of *Tg(pu1:Eos); Tg(gfap:NTR-mCherry)* and *Tg(pu1:Eos); Tg(nbt:DsRed)* animals demonstrating microglia that contain *gfap*[+] and *nbt*[+] debris. C. Quantifications of vacuoles inside individual microglia from 24h timelapse of *Tg(pu1:gfp)* animals. The number of vacuoles per microglia are scored every 5 minutes for 24 hours. D-E. The percentage of total microglia that transition between different vacuole-containing states (D) and the state of cells before their death (E) in 24h timelapse movies. F-G. Schematic of experimental design (F) and quantifications (G) to test the fate of microglia. Quantifications in G demonstrate the percentage of occurrences that 561-Eos[+] microglia in *Tg(pu1:eos)* results in 561-Eos[+] intact microglia, 561-Eos[+] microglia debris or 561-Eos[+] intact microglia and microglial debris 24, 48 and 72 hrs after labeling. H. Experimental paradigm schematic of experimental paradigm demonstrating that all microglia in the brain are labeled and then scored at 6 dpf. I. Quantification shows the percentage of microglia at 6 dpf that are labeled with 561-Eos and negative for 561-Eos (p<0.0001, unpaired t-test). Scale bar is 10 um (a,b). Additional supplemental material provided in Figure S2. Descriptive statistics represented in Table S1.

structures (Figure 2a). Transgenic animals for specific cell-types demonstrated the content of these vacuoles were astroglial (from *Tg(gfap:nsfb-mcherry)*)[25], neuronal (from *Tg(nbt:dsred)*)[12] and to a lesser extent oligodendroglial (from *Tg(sox10:mRFP)*)[26] debris (Figure 2b, S2a,e). By collecting images that spanned the brain, we identified that vacuole containing microglia represented the majority of microglia in the developing brain (Figure S2b, N=5 animals). We fate mapped these microglia by imaging them in the brain every 5 minutes for 24 hours and then tracked microglia and the vacuoles in them at every time point. Plotting each individual microglia in 24-hour periods demonstrated that microglia transitioned from non-vacuole containing to vacuole containing (Figure 2c). However, we could not detect microglia that transitioned from vacuole containing to non-vacuole containing over the 24-hour imaging period (Figure 2c,d, N=4 animals, n=12 cells). In these movies, we instead identified that all the microglia that died contained vacuole-like structures (Figure 2c,e, N=4 animals, n=10 cells), introducing the possibility that most embryonic microglia die before they completely digest efferocytic debris.

There seemed to be two simple hypotheses for these results: 1. either the completion of the digestion phase of microglia exceeds the 24-hour period or 2. developmental microglia die because they are mostly irreversibly vacuole containing. To explore these hypotheses, we tracked individual microglia over longer developmental periods. Using *Tg(pu1:eos)* animals, we photoconverted a single microglia that contained vacuoles per animal at 4 dpf, then imaged each animal in subsequent days (Figure 2f). After 24 hours, three outcomes occurred: 1. 27.78% of animals had only 561-Eos[+] debris in the brain, 2. 27.78% of animals had 561-Eos[+] debris and 561-Eos^{+} cells that contained vacuoles or 3. 44.44% of animals had 561-Eos^{+} cells that contained vacuoles, consistent with the idea that the microglia either died or divided (Figure 2g, N=18 animals). However, we could not detect 561-Eos[+] microglia that did not contain vacuoles. 3 days after photoconversion we rarely detected intact 561-Eos[+] microglia, but identified 561-Eos[+] debris in the brain (Figure 2g, N=18 animals). While it is possible that detection of Eos was compromised by time, we confirmed with a second transgenic line, *Tg(sox10:eos)*, that other long-lived cells, like dorsal root ganglia cells, could still be visualized 3 days after
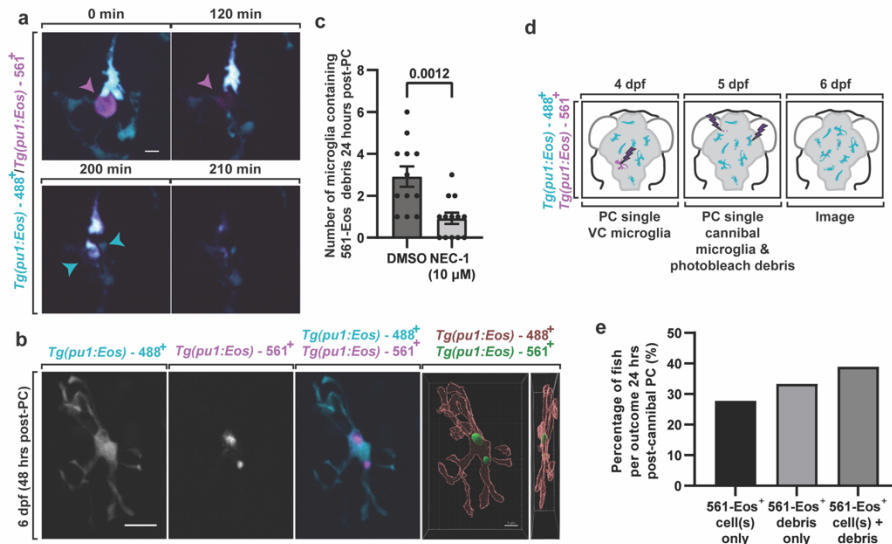
Figure 3. Microglia debris is cannibalized. A. Confocal images from 24h movie of *Tg(pu1:eos)* animals that had 561-Eos+ microglia that died and was cleared by 488-Eos+ microglia. Arrowheads denote a cell that undergoes death and is cannibalized. B. Confocal images of *Tg(pu1:eos)* at 24 hours after labeling of 561-Eos+ microglia showing 561-Eos+ microglia debris within 488-Eos+ intact microglia. C. Quantification of the amount of microglia that contained cannibalized 561-Eos+ debris in *Tg(pu1:eos)* animals treated with DMSO and Nec-1 for 24 hours (p=0.0012 DMSO vs Nec-1, unpaired t-test). D-E Schematic of experimental design (D) and quantifications (E) to determine the fate of cannibalistic microglia. Quantifications score the fate (561-Eos+ intact microglia, 561-Eos+ microglia debris or 561-Eos+ intact microglia and microglial debris) of cannibalistic microglia. Scale bar is 10 um (a,b). Descriptive statistics represented in Table S1.

photoconversion (Figure S2c,d, N=8 animals, n=48 cells). These data are consistent with the likelihood that once developmental microglia have vacuoles, they die within 3 days.

Microglia are thought to be long-lived cells that initially populate the brain during development[3]. Our results, however, indicate that once embryonic microglia become vacuole-containing in the zebrafish brain, they have short lifespans (Figure 2g, N=18 animals). Scoring of microglia from 3-5 dpf also showed 76.65% ± 1.95% of microglia are vacuole-containing on a given day (Figure S2b), and thus may be expected to die. Therefore, we next explored the scale of microglia death in the embryonic brain. To do this, we photoconverted all microglia in the brain of *Tg(pu1:eos)* animals at 3 dpf, and then scored the ratio of microglia that were photoconverted at 5 dpf (Figure 2h). These results indicated that on average 30.07% ± 4.81% of *pu1:Eos*+ cells in the brain were photoconverted (Figure 2i, N=11 animals, n=240 cells), supporting the idea that during peak stages of neural debris, microglia have short lifespans less than 3 days.

These results indicated that microglia debris is present when microglia are not only expanding but also the dominant phagocytic cell[3,12,20,27–31], at least of apoptotic debris. It is unclear how necroptotic debris would be removed in the embryo. Therefore, we next asked which cell-type was clearing microglia necroptotic debris. To do this, we searched the brain for microglia debris encased in the different phagocytic cells. We first assayed microglial debris in *Tg(pu1:RFP)*;*Tg(glast:GFPcaax-TA-nucRFP)*[32] and *Tg(pu1:GFP)*;*Tg(sox10:mrfp)*, which represent astroglia and neural crest/oligodendrocyte lineage cells that have been characterized as phagocytic[11,33,34]. However, we could not

detect microglia debris encased in either cell-type. We therefore devised a strategy to visualize microglia debris within living microglia by using our *Tg(pu1:eos)*-photoconversion paradigm to label microglia before they died and were cleared (Figure 1d). We then collected images of the brain 12 hours after photoconversion when 561-Eos+ microglia debris was present. In this paradigm, we detected 561-Eos+ microglia debris within 488-Eos+ microglia of all photoconverted animals (Figure 3a,b,c, N=12 animals), revealing the concept of microglia cannibalism (Figure 3b).

There were two likely hypotheses of how cannibalism occurred: 1. Microglia clear debris from dead microglia or 2. Microglia cannibalized portions of living microglia. To distinguish between these possibilities, we again labeled a random subpopulation of microglia with 561-Eos and tracked the appearance of microglia debris within migrating microglia in 24h time-lapse movies. In these movies, the majority of cannibalism events showed a sudden disappearance of fluorescence in the dying microglia corresponding with the arrival of other microglia that instantly had 561-Eos+ puncta consistent (Figure 3a). We did not detect microglia clearing of phagocytic cellular portions from other living microglia. If microglia necroptosis was the primary causative event for microglia cannibalism, then inhibiting microglia death should reduce the amount of microglia cannibalism. We therefore scored the amount of cannibalism in DMSO vs Nec-1 treated animals and detected that Nec-1 treated animals had less cannibalistic microglia than DMSO (Figure 3c)(p=0.0012 DMSO (N=12) vs NEC-1 (N=13), unpaired t-test), consistent with the hypothesis that microglia cannibalism is driven by microglia death. Taken together, this introduces a potential paradox that once developmental microglia become

phagocytic, they die, which produces debris that is eventually cannibalized by other microglia – such cannibalistic microglia are then vacuole-containing and thus may be expected to die, ultimately driving massive turnover of embryonic microglia.

To explore this paradox, we tracked embryonic microglia that were cannibalistic. In this paradigm, we first photoconverted individual microglia in *Tg(pu1:eos)* animals at 4 dpf and then selected animals at 5 dpf that had 561-Eos[+] debris inside 488-Eos[+] microglia but did not contain intact 561-Eos^{+} cells. We then bleached all the 561-Eos[+] debris in the brain of these animals, then photoconverted Eos to label the cannibalistic microglia with 561-Eos. 24 hours later, these animals were then scored for the presence of 561-Eos[+] debris and/or cells in the brain (Figure 3d,e, N=18 animals). We identified 33.33% of cannibalistic microglia generated 561-Eos[+] debris in the brain, 38.89% of cannibalistic microglia caused 561-Eos^{+} cells and 561-Eos[+] debris and 27.78% of cannibalistic microglia produced 561-Eos^{+} cells (Figure 3e, N=18 animals), consistent with the hypothesis that most cannibalistic microglia die.

We sought to further explore the paradox that most phagocytic microglia die, leading to debris that must be cannibalized, which then produces more phagocytic microglia that are destined to die (Figure 4a). Two predictions could be made based on that hypothesis, 1. decreasing microglia phagocytosis should reduce microglia debris and cannibalism and 2. increasing neural debris and thereby microglia phagocytosis should increase microglia

debris and cannibalism. We first reduced phagocytosis by treating *Tg(nbt:dsred); Tg(pu1:gfp)* animals with L-SOP, which inhibits phosphatidylserine-dependent phagocytosis that microglia utilize to clear dead neurons[21]. Animals treated with L-SOP from 4-5 dpf, had a reduced number of vacuole-containing microglia compared to DMSO-treated animals (Figure 4b)(DMSO (N=6 animals, n=132 cells), LSOP (N=6 animals, n=171 cells, p=0.0034 DMSO vs LSOP, unpaired t-test), confirming the treatment can inhibit phagocytosis[21]. L-SOP treated animals also had less GFP[+] microglial debris than DMSO (Figure 4c)(p=0.0005, DMSO (N=6 animals, n=132 cells), LSOP (N=6 animals, n=171 cells, unpaired t-test), indicating that inhibiting phagocytosis leads to less microglia death.

To test the paradox by increasing neural debris, we created injuries in the brain to non-microglia cells to generate more neural debris that is cleared by microglia. Injuries were created with a 532 nm single-pulsed laser[35–37]. As a sham-injury control, the 641 nm laser was exposed to a similar size injury site. We first established that our injury paradigm created neuronal debris in *Tg(nbt:dsred); Tg(pu1:eos)* by scoring the amount of *dsred*[+] puncta in the brain after the injury (Figure S3a). Despite an average of 4.667±12.69 neuronal *dsred*[+] debris per imaging window, the injury paradigm did not cause detectable 488-Eos[+] microglia debris immediately after the injury (Figure S3a,b)(N=6 animals, p<0.0001, dsRed[+] debris vs. Eos[+] debris, unpaired t-test). Consistent with the expansion of microglia after injury, 24 hours later we visualized an increase in microglia compared to
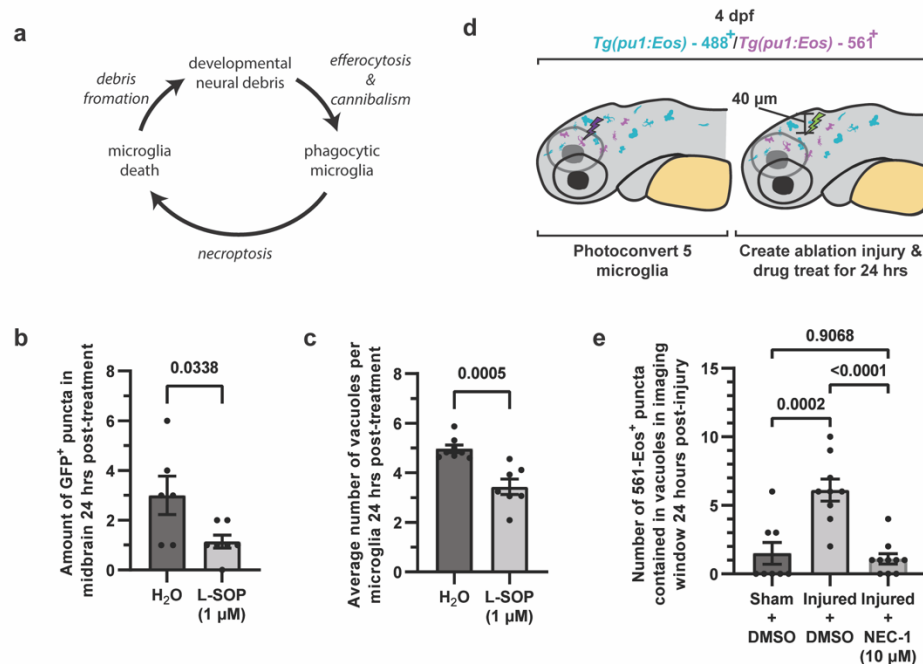
Figure 4. Phagocytosis and cannibalism shortens the lifespan of microglia. A. Schematic of the paradox that involves phagocytosis, necroptosis and cannibalism. B-C. Quantifications of the average number of vacuoles in microglia (B) (p=0.0338 H2O vs L-SOP, unpaired t-test) and amount of microglia debris in *Tg(pu1:gfp)* animals (C) treated with H2O (control) or L-SOP (p=0.0005, H2O vs L-SOP, unpaired t-test). D-E. Schematic of experimental design (D) and quantifications of cannibalistic microglia after laser-induced brain injury (E). Quantifications show the number of 561-Eos[+] puncta in 488-Eos[+] intact microglia 24 hours after sham injuries or laser- injuries in *Tg(pu1:Eos)* animals treated with DMSO or Nec1 for 24 hours after the injury (p=0.0002 Sham+DMSO vs Injured+DMSO, p<0.0001 Injured+DMSO vs Injured+Nec-1, p=0.9068 sham+DMSO vs injured+Nec-1, Post hoc Tukey test). Additional supplemental material provided in Figure S3. Descriptive statistics represented in Table S1.

sham-injured animals (Figure S3c)(Sham (N=5 animals) vs Injury (N=4 animals), p=0.0576, unpaired t-test). Having established the injury paradigm, we repeated it in *Tg(pu1:eos)* animals that had 5 microglia in the brain photoconverted and thereby labeled with 561-Eos[+] (Figure 4d). After 24 hours, we quantified that the number of 561-Eos[+] microglia debris present in the brain was in higher abundance in injured animals compared to sham-injured animals (Figure 4e)(Sham/DMSO (N=8) vs Injury/DMSO (N=9), p=0.0002, Post hoc Tukey test). The vast majority of this microglia debris was cannibalized by 488-Eos[+] microglia.

If the increase in microglia phagocytosis of neuronal debris is causing microglia to die, and thereby causing more microglia cannibalism, then blocking microglia death should reduce the amount of microglia debris and microglia cannibalism. We, therefore, tested if Nec-1 treatment reduced the number of cannibalistic microglia in the injury paradigm. In Nec-1 treated animals, the amount of 561-Eos[+] microglia debris returned to the level of sham-injured animals (Figure 4e)(Injury/Nec1 (N=10) vs Injury/DMSO (N=9), p<0.0001, Post hoc Tukey test). Microglia cannibalism also returned to the level of the uninjured animals, consistent with the hypothesis that phagocytic microglia death and cannibalism is dependent on necroptosis.

Together, our data shows that microglia that contain phagocytic debris in vacuoles have short lifespans that rarely exceed 3 days. Upon their death, developmental microglia debris is cannibalized by other microglia. The phagocytic nature of cannibalistic microglia then leads to their death and more debris that must be phagocytosed. This paradoxical process thereby establishes a cycle. This work, with others, establishes that microglia debris is cleared by astrocytes and microglia in specific contexts[11]. Beyond the universal principle that cells overexpand during development and then die via apoptosis[1,2], this work reveals an additional mechanism that produces developmental debris, induced by sacrificial microglia that function to clear apoptotic debris. Given the data here and evidence of necroptotic microglia in disease contexts[9,10], it will be intriguing to investigate if microglia cannibalism and a subsequent paradox that is driven by microglia cell death, is a hallmark of neuropathologies through ages.

AUTHOR CONTRIBUTIONS

ACKNOWLEDGEMENTS

COMPETING INTERESTS STATEMENT
The authors declare no competing interests.

REFERENCES:
1. Yamaguchi, Y. & Miura, M. Programmed cell death in neurodevelopment. *Developmental Cell* vol. 32 478–490 Preprint at https://doi.org/10.1016/j.devcel.2015.01.019 (2015).
2. Smith, C. J. Evolutionarily conserved concepts in glial cell biology. *Current Opinion in Neurobiology* vol. 78 Preprint at https://doi.org/10.1016/j.conb.2022.102669 (2023).
3. Paolicelli, R. C. *et al.* Microglia states and nomenclature: A field at its crossroads. *Neuron* **110**, 3458–3483 (2022).
4. Ginhoux, F. & Prinz, M. Origin of microglia: Current concepts and past controversies. *Cold Spring Harb Perspect Biol* **7**, 1–16 (2015).
5. Ginhoux, F. *et al.* Fate Mapping Analysis Reveals That Adult Microglia Derive from Primitive Macrophages. *Science (1979)* **330**, 841–845 (2010).
6. Ydens, E. *et al.* Profiling reveals two macrophage subsets with distinct localization , transcriptome and response to injury. *Nat Neurosci* (2020) doi:10.1038/s41593-020-0618-6.
7. Réu, P. *et al.* The Lifespan and Turnover of Microglia in the Human Brain. *Cell Rep* **20**, 779–784 (2017).
8. Zhan, L., Krabbe, G., Du, F., Jones, I. & Reichert, M. C. Proximal recolonization by self-renewing microglia re-establishes microglial homeostasis in the adult mouse brain. *PLoS Biol* 1–35 (2018).
9. Huang, Z. *et al.* Necroptosis in microglia contributes to neuroinflammation and retinal degeneration through TLR4 activation. *Cell Death & Differentiation 2018 25:1* **25**, 180–189 (2017).
10. Lloyd, A. F. *et al.* Central nervous system regeneration is driven by microglia necroptosis and repopulation. *Nat Neurosci* **22**, 1046–1052 (2019).
11. Zhou, T. *et al.* Microglial debris is cleared by astrocytes via C4b-facilitated phagocytosis and degraded via RUBICON-dependent noncanonical autophagy in mice. *Nature Communications 2022 13:1* **13**, 1–22 (2022).
12. Peri, F. & Nüsslein-Volhard, C. Live Imaging of Neuronal Degradation by Microglia Reveals a Role for v0-ATPase a1 in Phagosomal Fusion In Vivo. *Cell* **133**, 916–927 (2008).
13. Mazzolini, J. *et al.* Gene expression profiling reveals a conserved microglia signature in larval zebrafish. *Glia* **68**, 298–315 (2020).
14. Rovira, M. *et al.* Zebrafish Galectin 3 binding protein is the target antigen of the microglial 4C4 monoclonal antibody. *Dev Dyn* (2022) doi:10.1002/DVDY.549.
15. Slee, E. A. *et al.* Benzyloxycarbonyl-Val-Ala-Asp (OMe) fluoromethylketone (Z-VAD.FMK) inhibits apoptosis by blocking the processing of CPP32. *Biochem J* **315 (Pt 1)**, 21–24 (1996).
16. Green, L. A., O'Dea, M. R., Hoover, C. A., DeSantis, D. F. & Smith, C. J. The embryonic zebrafish brain is seeded by a

lymphatic-dependent population of mrc1+ microglia precursors. *Nat Neurosci* (2022) doi:10.1038/s41593-022-01091-9.

17. Sun, L. *et al.* Mixed lineage kinase domain-like protein mediates necrosis signaling downstream of RIP3 kinase. *Cell* **148**, 213–227 (2012).

18. Degterev, A. *et al.* Chemical inhibitor of nonapoptotic cell death with therapeutic potential for ischemic brain injury. *Nat Chem Biol* **1**, 112–119 (2005).

19. Dixon, S. J. *et al.* Ferroptosis: an iron-dependent form of nonapoptotic cell death. *Cell* **149**, 1060–1072 (2012).

20. Casano, A. M., Albert, M. & Peri, F. Developmental Apoptosis Mediates Entry and Positioning of Microglia in the Zebrafish Brain. *Cell Rep* **16**, 897–906 (2016).

21. Herzog, C. *et al.* Rapid clearance of cellular debris by microglia limits secondary neuronal cell death after brain injury in vivo. *Development (Cambridge)* **146**, (2019).

22. Weinlich, R., Oberst, A., Beere, H. M. & Green, D. R. Necroptosis in development, inflammation and disease. *Nat Rev Mol Cell Biol* **18**, 127–136 (2017).

23. Mazzoni, F. *et al.* Non-invasive in vivo fluorescence imaging of apoptotic retinal photoreceptors. *Sci Rep* **9**, (2019).

24. Eyo, U. B., Miner, S. A., Weiner, J. A. & Dailey, M. E. Developmental changes in microglial mobilization are independent of apoptosis in the neonatal mouse hippocampus. *Brain Behav Immun* **55**, 49–59 (2016).

25. Smith, C. J., Johnson, K., Welsh, T. G., Barresi, M. J. F. & Kucenas, S. Radial glia inhibit peripheral glial infiltration into the spinal cord at motor exit point transition zones. *Glia* **64**, 1138–1153 (2016).

26. Kucenas, S., Wang, W.-D., Knapik, E. W. & Appel, B. A Selective Glial Barrier at Motor Axon Exit Points Prevents Oligodendrocyte Migration from the Spinal Cord. *Journal of Neuroscience* **29**, 15187–15194 (2009).

27. Verney, C., Monier, A., Fallet-Bianco, C. & Gressens, P. Early microglial colonization of the human forebrain and possible involvement in periventricular white-matter injury of preterm infants. *J Anat* **217**, 436–448 (2010).

28. Xu, J., Wang, T., Wu, Y., Jin, W. & Wen, Z. Microglia Colonization of Developing Zebrafish Midbrain Is Promoted by Apoptotic Neuron and Lysophosphatidylcholine. *Dev Cell* **38**, 214–222 (2016).

29. Alexandria N. Hughes & Bruce Appel. Microglia phagocytose myelin sheaths to modify developmental myelination. *Nat Neurosci* (2020) doi:10.1016/j.expneurol.2008.09.010.

30. Paolicelli, R. C. *et al.* Synaptic pruning by microglia is necessary for normal brain development. *Science (1979)* **333**, 1456–1458 (2011).

31. Schafer, D. *et al.* Microglia sculpt postnatal neuronal circuits in an activivty and complement-dependent manner. *Neuron* **74**, 691–705 (2012).

32. Chen, J., Poskanzer, K. E., Freeman, M. R. & Monk, K. R. Live-imaging of astrocyte morphogenesis and function in zebrafish neural circuits. *Nat Neurosci* **23**, 1297–1306 (2020).

33. Zhu, Y. *et al.* Migratory Neural Crest Cells Phagocytose Dead Cells in the Developing Nervous System. *Cell* **179**, 74-89.e10 (2019).

34. Auguste, Y. S. S. *et al.* Oligodendrocyte precursor cells engulf synapses during circuit remodeling in mice. *Nature Neuroscience 2022 25:10* **25**, 1273–1278 (2022).

35. Green, L. A., Nebiolo, J. C. & Smith, C. J. Microglia exit the CNS in spinal root avulsion. *PLoS Biol* **17**, 1–30 (2019).

36. Nichols, E. L. & Smith, C. J. Functional Regeneration of the Sensory Root via Axonal Invasion. *Cell Rep* **30**, 9-17.e3 (2020).

37. Kikel-Coury, N. L. *et al.* Identification of astroglia-like cardiac nexus glia that are critical regulators of cardiac development and function. *PLoS Biol* **19**, e3001444 (2021).

38. Smith, C. J., Johnson, K., Welsh, T. G., Barresi, M. J. F. & Kucenas, S. Radial glia inhibit peripheral glial infiltration into the spinal cord at motor exit point transition zones. *Glia* **64**, 1138–1153 (2016).

39. Johnson, K. *et al.* Gfap-positive radial glial cells are an essential progenitor population for later-born neurons and glia in the zebrafish spinal cord. *Glia* **64**, 1170–1189 (2016).

40. McGraw, H. F., Snelson, C. D., Prendergast, A., Suli, A. & Raible, D. W. Postembryonic neuronal addition in Zebrafish dorsal root ganglia is regulated by Notch signaling. *Neural Dev* **7**, 23 (2012).

41. Kimmel, C., Ballard, W., Kimmel, S., Ullmann, B. & Schilling, T. Stages of Embryonic Development of the Zebrafish. *Developmental Dynamics* **203**, 253–310 (1995).

42. Nichols, E. L. & Smith, C. J. Pioneer axons employ Cajal's battering ram to enter the spinal cord. *Nat Commun* **10**, (2019).

43. Green, L. & Smith, C. J. Single-cell Photoconversion in Living Intact Zebrafish. *Journal of Visualized Experiments* e57024–e57024 (2018) doi:10.3791/57024.

44. Roca, F. J., Whitworth, L. J., Redmond, S., Jones, A. A. & Ramakrishnan, L. TNF Induces Pathogenic Programmed Macrophage Necrosis in Tuberculosis through a Mitochondrial-Lysosomal-Endoplasmic Reticulum Circuit. *Cell* **178**, 1344-1361.e11 (2019).

MATERIALS AND METHODS:
Contact for Reagent and Resource Sharing
All data collected for the study are included in the figures and supplemental data. Reagents are available from the authors upon request.

Experimental Model and Subject Details:
The University of Notre Dame IACUC which is guided by the United States Department of Agriculture, the Animal Welfare Fact (USA) and the Assessment and Accreditation of Laboratory Animal Care International approved all animal studies. Zebrafish strains in this study include: AB, *Tg(pu1:GAL4, UAS:GFP)*[zf149,12], *Tg(gfap:NTR-mCherry)*[sc059,38,39], *Tg(nbt:dsRed)*[zf148,12], *Tg(pu1:Eos)*[nt200,16], *Tg(sox10:Eos)*[w9,40], *Tg(sox10:mRFP)*[vu234,26], *Tg(slc1a3b:myrGFP-P2A-H2AmCherry)*[32], *Tg(pu1:GAL4, UAS:RFP)*[hdb2,12]. Only germline transgenic lines were used in this study. To produce embryos, pairwise matings were used. Animals were raised at 28°C in egg water in constant darkness and staged by hours or days post fertilization (hpf and dpf), confirmed by observation of developmental milestones[41]. Embryos were used for all experiments.

Method Details
In vivo imaging
Animals were anesthetized using 3-aminobenzoic acid ester (Tricaine), covered in 0.8% low-melting point agarose, and mounted dorsally in glass-bottomed 35 mm petri dishes[42]. A spinning disk confocal microscopes custom built by 3i technology (Denver, CO) that contains: Zeiss Axio Observer Z1 Advanced Mariana Microscope, X-cite 120LED White Light LED System, filter cubes for GFP and mRFP, a motorized X,Y stage, piezo Z stage, 20X Air (0.50 NA), 63X (1.15NA), 40X (1.1NA) objectives, CSU-W1 T2 Spinning Disk Confocal Head (50 μm) with 1X camera adapter, and an iXon3 1Kx1K EMCCD or Teledyne Prime 95B cMOS camera, dichroic mirrors for 446, 515, 561, 405, 488, 561,640 excitation, laser stack with 405 nm, 445 nm, 488 nm, 561 nm and 637 nm with laser stack FiberSwitcher, photomanipulation from vector high speed point scanner ablations at diffraction limited capacity, Ablate Photoablation System (532 nm pulsed laser, pulse energy 60J @ 200 HZ) was used to acquire images[42]. Images in time-lapse microscopy were collected every 5 min for 24 hours. Images were processed with Adobe Illustrator, ImageJ, and IMARIS. Only brightness and contrast were adjusted and enhanced for images represented in this study.

Immunohistochemistry
The primary antibody used in the confirmation of microglia debris in the brain was anti-4C4 (1:50, mouse, Seiger, Becker and Becker Laboratories)[13]. The secondary antibody used was Alexa Fluor 647 goat anti-mouse (1:600, Thermo Fisher, A-21235). Staining was performed using the protocol by Nichols and Smith[42]. Larvae were fixed at 3 dpf, 4 dpf, and 5 dpf in fresh 4% paraformaldehyde in 0.1% PBS Triton-X.
Photoconversion experiments

Single-cell photoconversions
Tg(pu1:eos) embryos were grown to 4 dpf. Pre-conversion confocal *z*-stack images were taken in the 488 nm/GFP filter set and 561 nm/RFP filter set to confirm there was no nonspecific photoconversion. Single, vacuole-containing *pu1*^{+} cells were then photoconverted using a 5-ms 405-nm-laser pulse guide to the midbrain with mVector (3i) in the midbrain at 4 dpf following the single-cell photoconversion protocol described in Green and Smith[43]. Following photoconversion, confocal *z*-stack images were taken in the 488 nm/GFP filter set and 561 nm/RFP filter set to confirm expression of the converted Eos[+] protein. Photoconverted animals were then grown to and imaged at 5 dpf, 6 dpf, and 7 dpf. Confocal 140 um *z*-stack images were taken of the dorsally mounted midbrains and the trunks of the fish were manually scanned for presence of 561eos cells and debris. We categorized the fish based on the presence of 561eos debris and 561 cells.

Cannibal tracking
Tg(pu1:eos) embryos were grown to 3 dpf. Pre-conversion confocal *z*-stack images were taken in the 488 nm/GFP filter set and 561 nm/RFP filter set to confirm there was no nonspecific photoconversion. Single, vacuole containing *pu1*^{+} cells were then photoconverted using a 5-ms 405-nm-laser pulse in the midbrain at 3 dpf following the single-cell photoconversion protocol above. Following photoconversion, post-conversion confocal *z*-stack images were taken in the 488 nm/GFP filter set and 561 nm/RFP filter set to confirm expression of the converted Eos[+] protein. Photoconverted animals were then grown to and imaged at 4 dpf. Confocal 140 um *z*-stack images were taken of the dorsally mounted midbrains and the trunks of the fish were manually scanned for presence of 561-Eos^{+} cells and debris. Fish with 561-Eos^{+} cells at 4 dpf were removed from the experiment. Cannibal microglia were identified as 488-Eos[+] microglia containing 561-Eos[+] debris in the remaining fish. One cannibal microglia was then selected per fish and photoconverted. All other 561-Eos[+] debris present was photobleached using as many 5-ms 561-nm-laser pulses as necessary. Fish were grown to and imaged at 5 dpf, 6 dpf, and 7 dpf. We categorized the fish based on the presence of 561-Eos[+] debris and 561-Eos^{+} cells.

Injury
Tg(nbt:dsRed);Tg(pu1:Eos) and *Tg(pu1:Eos)* 4 dpf animals were anesthetized using 0.02% 3-aminobenzoic acid ester (Tricaine) in egg water. Fish were then dorsally mounted in 0.8% low-melting point agarose solution, arranged laterally on a 10 mm glass-coverslip–bottom Petri dish, and placed on the microscope anterior to posterior. Injured were performed in the midbrain. Specific site of laser-induced injury was determined by bringing the skin of the fish above the brain into focus and using the piezo Z stage to move 40 μm below the surface of the skin. This area was marked and brought into a focused ablation window. Upon focusing the targeted region, we double-clicked on a *dsRed*[+] region using a 4 μm cursor tool. All laser parameters used are specific to our confocal microscope. Specific parameters include Laser Power (1), Raster Block Size (1), Double-Click Rectangle Size (4), and Double-Click Repetitions (4). After injury, fish were released from the agarose and treated with 1% DMSO or Nec-1. Sham-injured fish were followed the same procedure but were expose to single pulses of 561 nm laser with mvector rather than the Ablate! Laser.

Chemical treatments
Cell death inhibitors
The chemical reagents used were Z-VAD-FMK[15], Ferrostatin-1 (Fer-1; Sigma, SML0583)[19], Necrostatin-1 (Nec-1; MedChemExpress LLC, HY-15760)[18], Necrosulfamide (NSA; Tocris Bioscience)[17]. Stock solutions of 20 mM Z-VAD-FMK, 2.5 mM Fer-1, 10 mM Nec-1, and 10 mM NSA were stored at −20°C dissolved in DMSO. Working solutions were diluted with PTU to 20 μM for Z-VAD-FMK treatments, 2.5 μM for Fer-1 treatments, 10 μM for Nec-1 treatments[44], and 20 μM for NSA treatments. All embryos were incubated in egg water until 24 hpf and incubated with PTU until desired treatment time. Fish were treated at 4 dpf, immediately after photoconversions. Control fish were incubated with 1% DMSO in PTU.

L-SOP treatment
The chemical reagent used for this study was O-Phospho-L-serine (L-SOP; Sigma, P0878-10MG). Stock solutions were dissolved in H_2O to a concentration of 1 mM. Working solutions were diluted to 1 μM with PTU[21]. All embryos were incubated in egg water until 24 hpf and incubated with PTU until desired treatment time. Fish were bathed at 4 dpf with 10 μM L-SOP dissolved in egg water for 24 hours. Control fish were incubated with H_2O.

PSVue Labeling
For imaging determining if microglia express phosphatidyl serine, embryos were bathed in a 1:250 solution of PSVue® 643 (PSVue; Polysciences, Inc.) diluted in egg water for 1 hour prior to imaging.

Quantification and statistics
3i Slidebook software was used to generate composite z-stack images of microglia. All individual z-stack images were sequentially observed. IMARIS (Notre Dame Imaging Core) was used to create 3D surface renderings of microglia. All graphical data represent both the mean and individual values used in each experiment unless otherwise noted. All quantifications were performed using various plug-ins available in FIJI (ImageJ) and Microsoft Excel. GraphPad Prism (version 8) software was used to perform all statistical analysis.

No statistical methods were used to predetermine sample sizes, however all sample sizes are informed by previous publications. All statistical tests were run with biological replicates, not technical replicates. Healthy animals were randomly selected for experiments. No data points were excluded from analysis. Data distribution was assumed to be normal, but this was not formally tested. Unless otherwise indicated, data collection and analysis were performed blind to the conditions of the experiments. Each experiment was repeated at least twice with similar results.

Quantification of debris
GFP+ debris, 488-Eos+ debris, 561-Eos+ debris, *gfap*+ debris, *nbt*+ debris, and *sox10*+ debris were counted manually in Slidebook and ImageJ across all consecutive images in *z*-stacks of the midbrain. 488-Eos+ microglia were considered cannibalistic if they contained 561-Eos+ debris.

Quantification of vacuoles
24 hour timelapse movies were taken of 4 dpf *Tg(pu1:GAL4; UAS:GFP)* fish. Individual microglia were manually tracked at every 5 minute timepoint of the timelapses. At each timepoint, the number of vacuoles an individual microglia contained was counted by going through images in *z*-stacks and was supported by the use of Slidebook's 4D volume view feature. Vacuoles were counted at every timepoint until the microglia left the capture window. Vacuoles were defined as GFP- inclusions of any size that were completely contained within GFP+ microglia.

Cell morphology quantifications
Analysis of microglia area and roundness were used to describe changes in microglia morphology. Microglia area and roundness were measured at every 5-minute time point before death using the trace feature on ImageJ. ImageJ calculates roundness using the formula:

$$Roundness = \frac{4 \times area}{\pi \times (major\ axis)^2}$$

IMARIS
3D surface reconstructions were generated using IMARIS. The surface tool was use to generate surface renderings from confocal stacks taken with 1 um step sizes. Only brightness and contrast were adjusted.
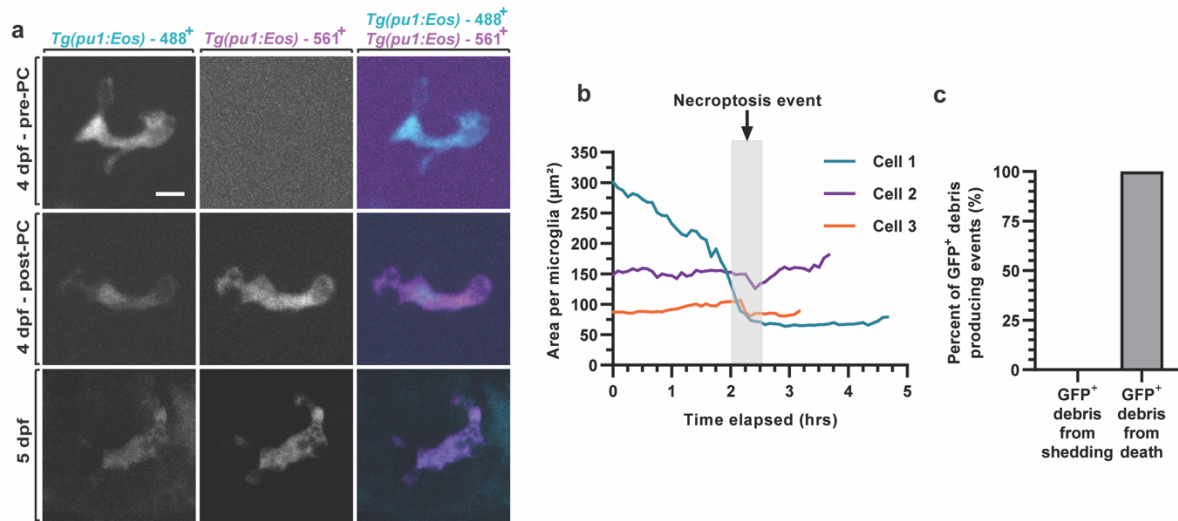
Softwares
ImageJ and Slidebook were used to produce and process confocal images. Graphpad prism was used to generate all graphs and statistical analysis. Adobe Illustrator was used to compile the figures and p1.

DATA AVAILABILITY:
All data collected for this study are included in the figures and supplementary material.
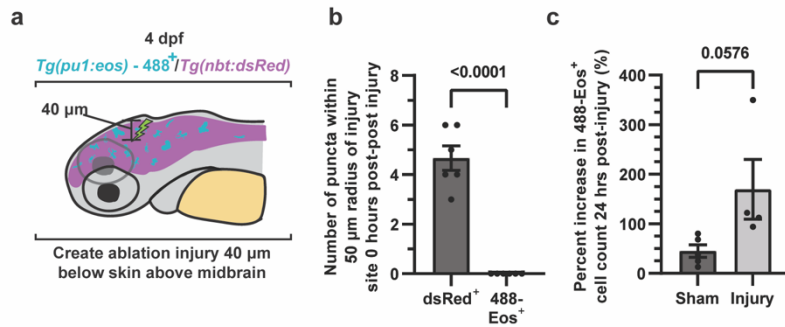
SUPPLEMENTAL FIGURES

Figure S1. Supplemental material for Figure 1. A. Images from a confocal microscope of 4 dpf *Tg(pu1:Eos)* animals before and after exposure to 405 nm. Note that absence of *Tg(pu1:Eos) -561*[+] before photoconversion. B. Quantification of the area of microglia during cell death event. Note that cells rapidly decrease area just before the necroptosis event. C. Quantification of the amount of debris causing events that result from shedding vs cell death in 24-hour timelapse movies of 4 dpf *Tg(pu1:GFP)* animals. Descriptive statistics represented in Table S1.
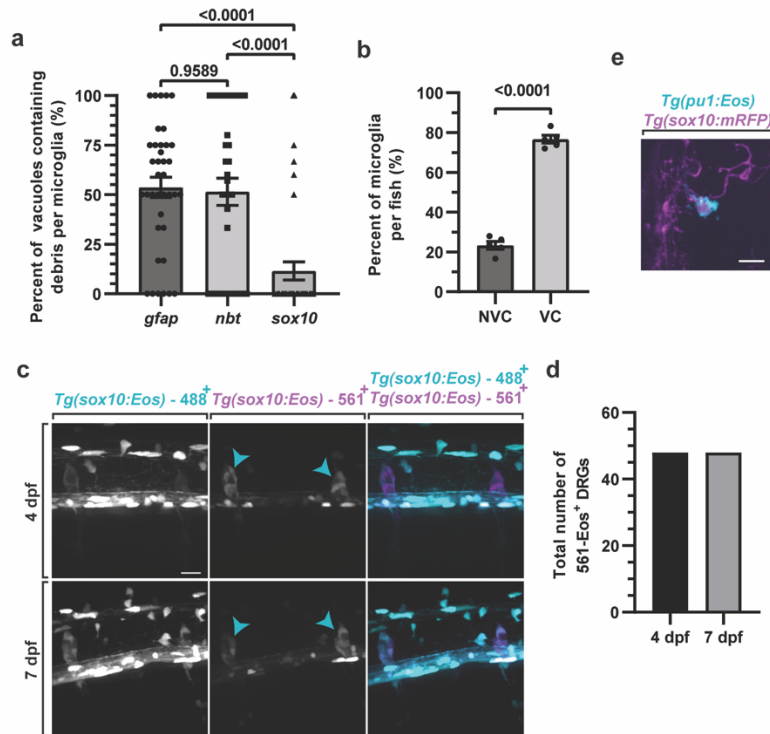
Figure S2. Supplemental material for Figure 2. A. Quantification of the percentage of vacuoles in microglia that enclose each type debris from *Tg(gfap:nsfb-mcherry), Tg(nbt:DsRed)* and *Tg(sox10:mRFP)* animals (p=0.9589 *gfap* vs *nbt*, p<0.0001 *gfap* vs *sox10*, p<0.0001 *nbt* vs *sox10,* Post hoc Tukey test). B. Quantification of the percentage of microglia per 4 dpf animals that are non-vacuole (NVC) vs vacuole containing (VC)(p<0.0001 NVC vs VC, Fisher's exact test). C. Confocal images of *Tg(sox10:Eos)* animals that were photoconverted at 4 dpf and imaged at 4 and 7 days, demonstrating the Eos photoconversion is stably detected at least 3 days after photoconversion. D. Quantifications from C that demonstrate that photoconversion causes stable labeling of Eos+ cells. Descriptive statistics represented in Table S1.

Figure S3. Supplemental material for Figure 4. A. Schematic demonstrating how injuries were created and calibrated in animals. B. Quantification of the amount of debris immediately after injury from Tg(*nbt:DsRed)*[+] vs *Tg(pu1:Eos)*^{+} cells in the injury paradigm ($p < 0.0001$ dsRed[+] vs 488-Eos[+], unpaired t-test). C. Quantification of the percentage increase in *Tg(pu1:Eos)*^{+} cells in animals 24 hours after sham or injury ($p = 0.0576$ sham vs injury, unpaired t-test). Note the microgliosis consistent with focal brain injuries. Descriptive statistics represented in Table S1.

Table S1. Table of Descriptive Statistics. Table that presents the descriptive statistics for every figure panel that presents quantifications.

Movie S1. Microglia cannibalism. Confocal images of a 24 hour timelapse of 4 dpf *Tg(pu1:Eos)* animals that had photoconverted microglia demonstrating a 561-Eos[+] cell that dies and is cannibalized by 488-Eos[+] cell.